Int J Clin Exp Med 2017;10(12):16004-16026
www.ijcem.com /ISSN:1940-5901/IJCEM0068660

Original Article

Classification of MRI and psychological testing data based on support vector machine

Wenlu Yang[1], Xinyun Chen[1], David S Cohen[2], Eric R Rosin[2], Arthur W Toga[3], Paul M Thompson[3], Xudong Huang[2], For the Alzheimer's Disease Neuroimaging Initiative[*]

[1]Department of Electrical Engineering, Information Engineering College, Shanghai Maritime University, Shanghai, China; [2]Neurochemistry Laboratory, Department of Psychiatry, Massachusetts General Hospital and Harvard Medical School, Charlestown, MA, USA; [3]Laboratory of Neuro Imaging, The Mark and Mary Stevens Neuroimaging and Informatics Institute, Keck School of Medicine of USC, University of Southern California, Los Angeles, CA, USA; [*]Data used in preparation of this article were obtained from the Alzheimer's Disease Neuroimaging Initiative (ADNI) database (adni.loni.usc.edu). As such, the investigators within the ADNI contributed to the design and implementation of ADNI and/or provided data but did not participate in analysis or writing of this report. A complete listing of ADNI investigators can be found at: http://adni.loni.usc.edu/wpcontent/uploads/how_to_apply/ADNI_Acknowledgement_List.pdf.

Received November 6, 2017; Accepted November 21, 2017; Epub December 15, 2017; Published December 30, 2017

Abstract: Alzheimer's disease (AD) is a progressive, and often fatal, brain disease that causes neurodegeneration, resulting in memory loss as well as other cognitive and behavioral problems. Here, we propose a novel multimodal method combining independent components from MRI measures and clinical assessments to distinguish Alzheimer's patients or mild cognitive impairment (MCI) subjects from healthy elderly controls. 70 AD subjects (mean age: 77.15 ± 6.2 years), 98 MCI subjects (mean age: 76.91 ± 5.7 years), and 150 HC subjects (mean age: 75.69 ± 3.8 years) were analyzed. Our method includes the following steps: pre-processing, estimating the number of independent components from the MR image data, extracting effective voxels for classification, and classification using a support vector machine (SVM)-based classifier. As a result, with regards to classifying AD from healthy controls, we achieved a classification accuracy of 97.7%, sensitivity of 99.2%, and specificity of 96.7%; for differentiating MCI from healthy controls, we achieved a classification accuracy of 87.8%, a sensitivity of 86.0%, and a specificity of 89.6; these results are better than those obtained with clinical measurements alone (accuracy of 79.5%, sensitivity of 74.0%, and specificity of 85.1%). We found that (1) both AD patients and MCI subjects showed brain tissue loss, but the volumes of gray matter loss in MCI subjects was far less, supporting the notion that MCI is a prodromal stage of AD; and (2) combining gray matter features from MRI and three commonly used measures of mental status, cognitive function improved classification accuracy, sensitivity, and specificity compared with classification using only independent components or clinical measurements.

Keywords: Alzheimer's disease, mild cognitive impairment, structural MRI, source-based morphometry, independent component analysis, support vector machine

Introduction

The most common form of dementia, accounting for 50% to 80% of dementia cases, is Alzheimer's disease (AD). AD is a progressive, and often fatal, brain disease that causes neurodegeneration, resulting in memory loss as well as other cognitive and behavioral problems that are often severe enough to affect all aspects of a person's life. Effective and valid early diagnosis is vital for the slowing and, ultimately, the prevention of disease progression. A variety of biomedical imaging techniques such as structural or functional magnetic resonance imaging (sMRI/fMRI) [1-10] and positron emission tomography (PET) [11-14] are being used to assess AD patients. sMRI is a noninvasive and efficient technology, and plays an important role in the diagnosis of AD. Many studies have manually or semi-automatically measured various a priori brain regions of interest (ROI) [3, 15-20], because compared to healthy controls (HC), AD patients have substantial cerebral atrophy. ROI analysis focuses on specific brain regions, especially the hippocampus and entorhinal cortex [21-24]. By comparing regional volumes of ROIs across diagnostic groups, researchers have uncovered valuable information about the patterns of morphometric differences, and have laid the foundation for subsequent studies for which voxel-based morphometry (VBM) [25, 26] and tensor-based morphometry (TBM) [27] are widely used methods to calculate tissue changes with mathematically complex voxel-wise modeling [28, 29]. ROI-based analyses falls short in several respects: first, they typically only consider a spatially limited region of the subject's brain, neglecting much of the available information, which may be important [30]. Second, when univariate analyses are used, they are incapable of including the joint information among voxels in a 3D image and are often less effective at analyzing individual subjects. Although largely prevalent in univariate tests, some multi-ROI studies have been done.

By contrast, multivariate methods consider the relationship among voxels; they may also consider volumes of several prior regions of interest, segmented manually or automatically. Voxels with a similar attribute may be aggregated into one group, and all of these voxels make up a source. Inspired by the source concept, source-based morphometry (SBM) [31, 32] was developed from VBM with four key steps: preprocessing, ICA, statistical analysis, and statistical mapping. Before we actually perform ICA as a requirement of SBM, we need to estimate the number of independent components. This involves testing the eigenvalues of a sample covariance matrix in order to estimate the number of the equal smallest eigenvalues of the true covariance matrix that is based on the information theoretic criterion (ITC) [33].

Classifying patients as AD versus normal is also a major goal in the diagnosis of AD. We begin by describing how to extract features from different groups of subjects. In diverse applications across various fields, support vector machines (SVMs) turn out to be one of the most effective feature extraction methods [34-38] that can be mathematically simplified using optimization techniques [39].

In this paper, we first describe the methods used in our experiments and the cohort studied in the Methods section. Results of our analyses are detailed in the results section, followed by a discussion and conclusion.

Materials and methods

Magnetic resonance images

Data used in the preparation of this article were obtained from the Alzheimer's Disease NeuroimagingInitiative (ADNI) database (adni.loni.usc.edu). The ADNI was launched in 2003 as a public-private partnership, led by Principal Investigator Michael W. Weiner, MD. The primary goal of ADNI has been to test whether serial magnetic resonance imaging (MRI), positron emission tomography (PET), otherbiological markers, and clinical and neuropsychological assessment can be combined to measure the progression of mild cognitive impairment (MCI) and early Alzheimer's disease (AD).

The MRI data used in this paper is from the Alzheimer's Disease Neuroimaging Initiative (ADNI), which has recruited over 800 adults, aged 55 to 90, from 55 initially planned sites across the United States and Canada [40] (later extended to 59 sites) [41]. In the initial stage of the study, approximately 200 cognitively normal individuals were followed for three years; 400 subjects with MCI were followed for three years; and 200 patients with early AD were followed for two years. Later on, these time periods were extended and more subjects were added [42]. Quality control procedures were applied to ensure that the correct scan protocol, orientation, and angulations were used [40]. ADNI data has been classified using SVMs in the past [43].

In our study we chose the 1.5 T T1-weighted MRI screening scans that can be used as baseline scans for our following research subjects with the MRIs in which extreme detected deformations were excluded. We randomly picked MRIs and constructed three groups of MRIs: group AD included 70 MRI images of AD patients, group MCI was composed of 98 subjects with MCI, and 150 cognitively normal individuals' MRIs were included in group HC. Each group of MRI gray matter images, segmented from the MRI data [35], shared a similar number of voxels that could clearly be distinguished from an MRI viewer like MRIcro [44], which offers a mean image after preprocessing. Those images with a largely deviated number of voxels were abandoned in advance to improve classification. The final smoothed gray matter images with voxel dimensions of $3 \times 3 \times 3$ mm^3 had all gone through a series of preprocessing of normalization, interpolation, and smoothing

Table 1. Simulation results of MDL and MIC

k	1	2	3	4	5	6
Test 1: q = 2						
MDL	34.738	35.7737	43.8276	52.3569	58.3623	62.1698
MIC	43.6486	42.4132	47.3038	52.3559	57.6437	63.4953
Test 2: q = 2 (The position of sources were changed)						
MDL	150.1347	38.6703	45.7595	53.2579	59.0382	62.1698
MIC	150.1087	43.3698	47.6558	52.913	58.326	63.4953
Test 3: q = 3						
MDL	499.7452	78.2846	47.6271	53.5419	58.8385	62.1698
MIC	483.2545	76.4261	47.7218	52.38	57.8054	63.4953

using the SPM8 toolbox that we will discuss later in the preprocessing section. Our goal was to compare AD images with HC ones, and MCI images with HC images, respectively, and draw out features from these comparisons. A brief summary of the participants' demographics and dementia status is listed in **Table 2**. This table demonstrates the participants' statistical gender, age, education, socioeconomic, and clinical dementia rating information. The number of participants in each group is listed in column Num. Corresponding columns show the mean value of the mini-mental state examination (MMSE), the age and weight of these three groups, and the number of people with the specific scale value of GDS total score (GDSCALE), CDR, Modified HachinskiIschaemic scale (HMSCORE), and sex.

Overview

Information theory criteria overview: We intended to use SBM to study MR image data, which involves the procedure of ICA; however, to avoid choosing the number of independent components randomly and arbitrarily, we calculated the number by a principle method. A commonly used ITC for order selection [45], AIC [46], is developed based on the minimization of the Kullback-Leibler divergence between the true model and the fitted model. AIC is extended by Cavanaugh as the Kullback-Leibler information criterion (KIC) [47] using a symmetric Kullback-Leibler divergence between the true and fitted models. MDL criterion is developed based on the minimum code length.

Although these two approaches have similar structures, each of them has their own specialties [48-50]. AIC has the advantage of performing well for those "difficult" problems when large eigenvalues are not much bigger than the smallest eigenvalues, but is inconsistent and tends to overestimate the model order for the easier cases. MDL on the other hand, performs with extreme reliability for most cases but falls short of AIC's performance for difficult cases [51]. Here, we come up with a question: is there any approach that can leverage both criterions' advantages without also absorbing their disadvantages?

The minimum probability of error criterion (introduced by Douglas B. Williams [48]) based on the theory of multiple hypothesis tests, performs better than either AIC or MDL. Here, we call this approach modified ITC, and symbolize it as MIC. The equation for MIC can be summarized as equation 1:

$$\mathrm{MIC}(k) = -\frac{1}{2}(T-k)(n-k)\log\left(\frac{\prod_{i=k+1}^{T}\lambda_i^{\frac{1}{T-k}}}{\frac{1}{T-k}\sum_{i=k+1}^{T}\lambda_i}\right) + \frac{k}{4}(2T-k-1)\log\frac{n}{2} - \log\left(\pi^{-\frac{p(p+i)}{4}}\Gamma_k\left(\frac{T}{2}\right)\right) - \sum_{i=1}^{k}\sum_{j=k+1}^{T}\frac{1}{2}\log\frac{\lambda_i-\lambda_j}{\lambda_i\sigma^{-2}} + \sum_{j=k+1}^{T}\sum_{k=j+1}^{T}\log\frac{(\lambda_j\lambda_k)^{1/2}}{\lambda_j-\lambda_k} \qquad (1)$$

In this equation, n is one less than the number of samples and $\sigma^{-2} = \frac{1}{T-k}\sum_{i=k+1}^{T}\lambda_i$, $\Gamma_k(a)$ is the multivariate gamma function. To testify the availability of MIC compared to MDL, we make use of the resulting eigenvalues of Mati Wax and Thomas Kailarth's simulation [33] in which seven sensors specifically receive data sent by several sources in different directions and are independently distributed. A hundred samples are extracted from each sensor so that N=100. The number of signal sources (the value of q) is changed to see whether or not MDL and MIC can correctly offer a corresponding estimation of the source number. The results of these tests are displayed in **Table 1**.

From Test 1, MIC reached a minimal value when k was 2, while MDL was smallest when k was 1. The reason why MDL, in this case, missed the right source number, is that this case is what we called a "difficult case" and it is one, like we

Table 2. The summary of participants' clinical status

Group	Num.	MMSE	GDSCALE (0/1/2/3/4/5/6)	CDR (0/0.5/1)	HMSCORE (0/1/2/3/4)	Age	Weight	Sex (F/M)
AD	70	22.96 ± 1.9	15/20/15/8/9/2/1	0/24/46	26/38/3/3/0	77.15 ± 6.2	72.32 ± 12.0	30/40
MCI	98	26.95 ± 1.5	16/32/21/14/9/6/0	0/98/0	37/52/4/4/1	76.91 ± 5.7	76.35 ± 11.9	39/59
HC	150	29.17 ± 0.7	79/41/17/8/4/1/0	150/0/0	84/59/3/4/0	75.69 ± 3.8	75.63 ± 12.7	67/83

mentioned above, with which MDL is ineffective. In Test 2, the position of those two sources was regulated and both criterions received the correct number of 2. In Test 3, one more source was added and after the same calculation.

From the results of the three simulations, MIC could correctly identify the right number of sources that we set. MDL failed in Test 1 to expose a shortcoming that needs to be avoided. Although we cannot directly conclude that MIC performs better than AIC in these three simulations, we can say that MIC and MDL share more similarity than MIC and AIC, and that this similarity will guarantee that MIC, like MDL, performs more stably over most cases that would be certified in the following experiment with the subject data. As a result, we decided to use MIC during our study to estimate the independent components before we actually carried out ICA.

SBM overview

Deformation-based morphometry (DBM) and TBM are two computational neuro-anatomical methods for studying brain shapes based on deformation fields obtained by the nonlinear registration of brain images. When comparing groups, DBM uses deformation fields to identify differences in the relative positions of structures within subjects' brains. TBM can refer to those methods that localize the differences in the local shapes of brain structures and can be used to produce statistical parametric maps of regional shape differences.

VBM is another class of techniques that can be applied to some scalar function of the normalized image. When VBM is compared with TBM at small scales that need to compute very high resolution deformation fields, it is simple and pragmatic in addressing small-scale differences [28, 29]. Simply speaking, VBM involves a voxel-wise comparison of the local concentration of gray matter between two groups of subjects. Although these earlier morphometric measurements resulted in a wealth of findings pertaining to some particular cases,a number of morphometric features may be more difficult to quantify by inspection. While the VBM approach is not biased to one particular structure, it even-handedly and comprehensively assesses anatomical differences throughout the brain.

Compared to VBM, which involves the process of pre-processing, statistical analysis, and statistical maps, SBM [31] derived from VBM also includes ICA between the pre-processing step and the statistical analysis step as shown in **Figure 1**.

With VBM, the procedure is quite straightforward and generally involves the following two steps: first, in the pre-processing step it spatially normalizes high-resolution images from all the subjects into the same stereotactic space that is followed by segmenting the gray matter from the spatially normalized images and smoothing the gray-matter segments. Second, to do the statistical analysis, voxel-wise parametric statistical tests comparing the smoothed gray matter images from the groups are performed. Corrections for multiple comparisons are made using the theory of Gaussian random fields.

Identical to VBM, SBM applies the same process in the pre-processing step and the statistical analysis step with the only difference being that it carries out ICA. ICA is a statistical and computational technique for revealing hidden factors that underlie sets of random variables, measurements, or signals, before performing statistical analysis. ICA defines a generative model for the observed multivariate data that is typically given a large database of samples and, in the model, the data variables are assumed to be linear or a nonlinear mixture of some unknown latent variables; the mixing system is also unknown. The latent variables, called the independent components, sources, or factors, are assumed non-Gaussian and mutually independent, and can be found by ICA. As a result, ICA performed here can identi-

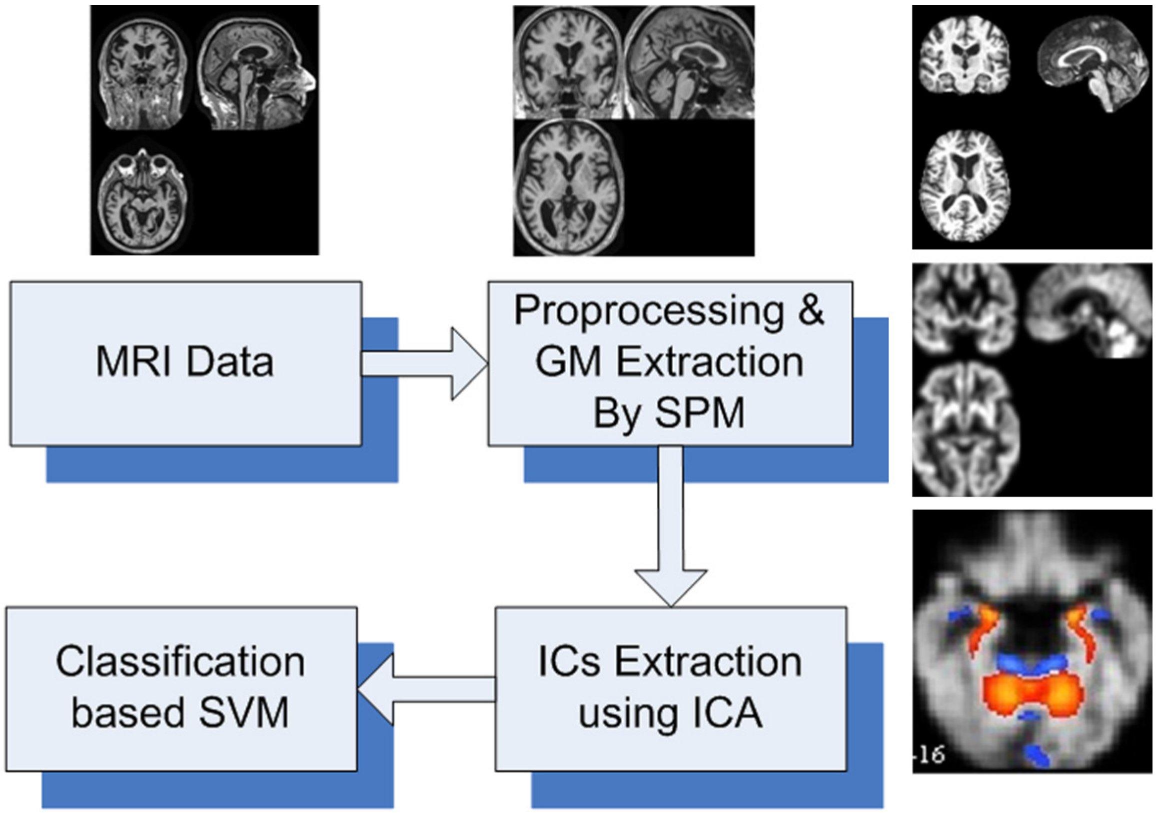

Figure 1. The framework of the whole processing. First, all MR images are normalized into a template, then segmented and smoothed. Next, the normalized gray matter images are analyzed using ICA. Finally, features extracted based on ICA are fed into a SVM-based classifier for the diagnosis of individuals as AD, MCI, or HC subjects.

fy the potentially natural implicit groupings in the data that possess the target of our study to determine the significantly differentiating natures among groups.

Procedure

The whole procedure of the analysis is summarized in **Figure 1**. Following the procedure described above, we performed the analysis of the MRI data. All the gray matter images of 70 AD patients, 98 MCI subjects, and 150 healthy subjects were divided into three different groups, labeled AD, MCI and HC, respectively.

Preprocessing

As we discussed before, pre-processing is the basis of our subsequent analysis and calculation [52]. We conducted pre-processing using Matlab toolbox SPM8 [53] that, on one hand, is used to realize the unification of brain volume in order to locate a specific voxel of different images in the same spatial position. On the other hand, it is used to increase the SNR of the data and eliminate the nuances among different subjects' brain structures. First, we realigned all images using a least squares approach and a six-parameter (rigid body) spatial transformation. Then we spatially normalized MRI images into a standard space defined by the T1 template image that conforms to the space defined by the ICBM, NIH P-20 project and is approximate to that space described in the atlas of Talairach and Tournoux [54]. After the rough normalization, all the images were smoothed with a Gaussian kernel to suppress anatomical noise and affects. Lastly, we extracted gray matter images by segmentation. All the subsequent processes were applied to the gray matter images segmented from the MRI data [35].

Independent component estimation

Since we have pre-processed the images into gray matter images, we came to the next processing stage: ICA. Here we separate the ICA processing step into two parts [55]. One is

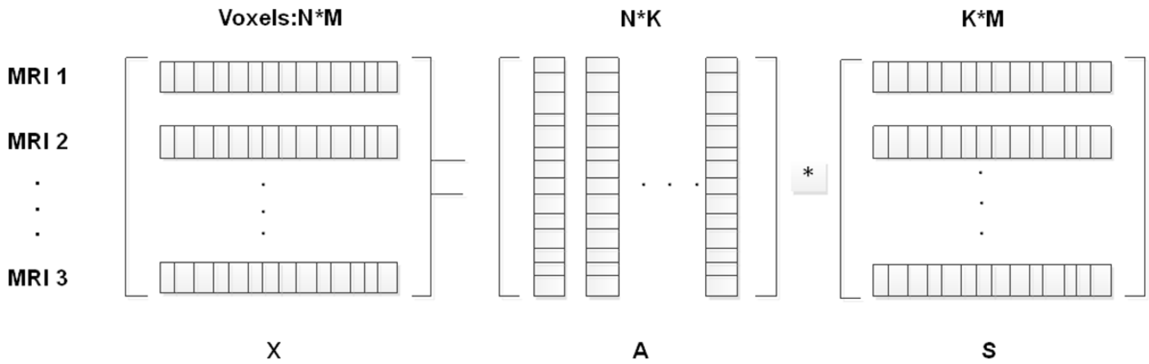

Figure 2. A model of ICA. Each row of matrix X represents the voxel values from one MRI and after the decomposition mixing matrix A and source matrix S come into being. Each column of A can be figured as one component composite of information of all MRIs, and each row of S with the same number of voxels in one specific MRI can be used to realize the visualization of the component.

the independent components estimation that should be carried out beforehand, and the other is the specific ICA that we usually mean when we speak of ICA [56]. There is another MATLAB toolbox, called GIFT [31, 57], that we found to be quite useful in our analysis. It is often used to perform Group ICA of functional MRI images. With plenty of reliable and useful programs integrated into it, GIFT is an excellent reference library.

To estimate the number of independent components, we used the modified MIC that was described in the analysis above. We sub-sampled the data matrix of gray matter images to generate an independently and identically distributed (IID) image set for the component estimation. The judgment of whether the dataset meets the IID requirement is made by calculating the entropy rate and comparing it to the entropy rate of an IID Gaussian random process of the same variance and data length. Once the entropy rate reaches that threshold value, the data can be viewed to meet the IID requirements. Then the MIC can be applied.

We used the estimated number of independent components as one input parameter of ICA. Here, we realize that it is necessary to have a simple, but clear, understanding of ICA.

Independent components analysis

ICA defines a generative model for the observed multivariate data [58-60] in which the data variables are assumed to be a linear or nonlinear mixture of some unknown latent variables, and the mixing system is also unknown. The latent variables are assumed non-Gaussian and mutually independent, and they are called the independent components of the observed data. ICA is typically modeled as Equation 2.

$$X = A \times S \tag{2}$$

The model is also demonstrated in **Figure 2** in which X represents the observed multivariate data. Each row of X is resized from one image so that the number of columns is equal to the number of voxels in one image. X is decomposed into mixing matrix A and source matrix S. Each row of A consists of all the independent components in one image, while each column of A is equivalent to one component of all images. The source matrix S, which contains the information of voxels, can be used to reconstruct images.

Component analysis

We run the two-sample t-test the way we had conceived above, and we get the components that we need. The *p*-value we set in order to determine the choice of components was 0.05, which is a typical threshold value in a two-sample t-test [61-63]. As mentioned before, matrix S holds the related information between voxels and components, so it can be used to realize the visualization of those components we have extracted. To do it, every row of source matrix was reshaped into a 3D image, scaled to the unit standard deviation, and fit in a threshold at $|z| > 3.0$. Then, the images of the components that we have chosen were overlaid on the normalized template image [64]. We could also transform the coordinates of the significant

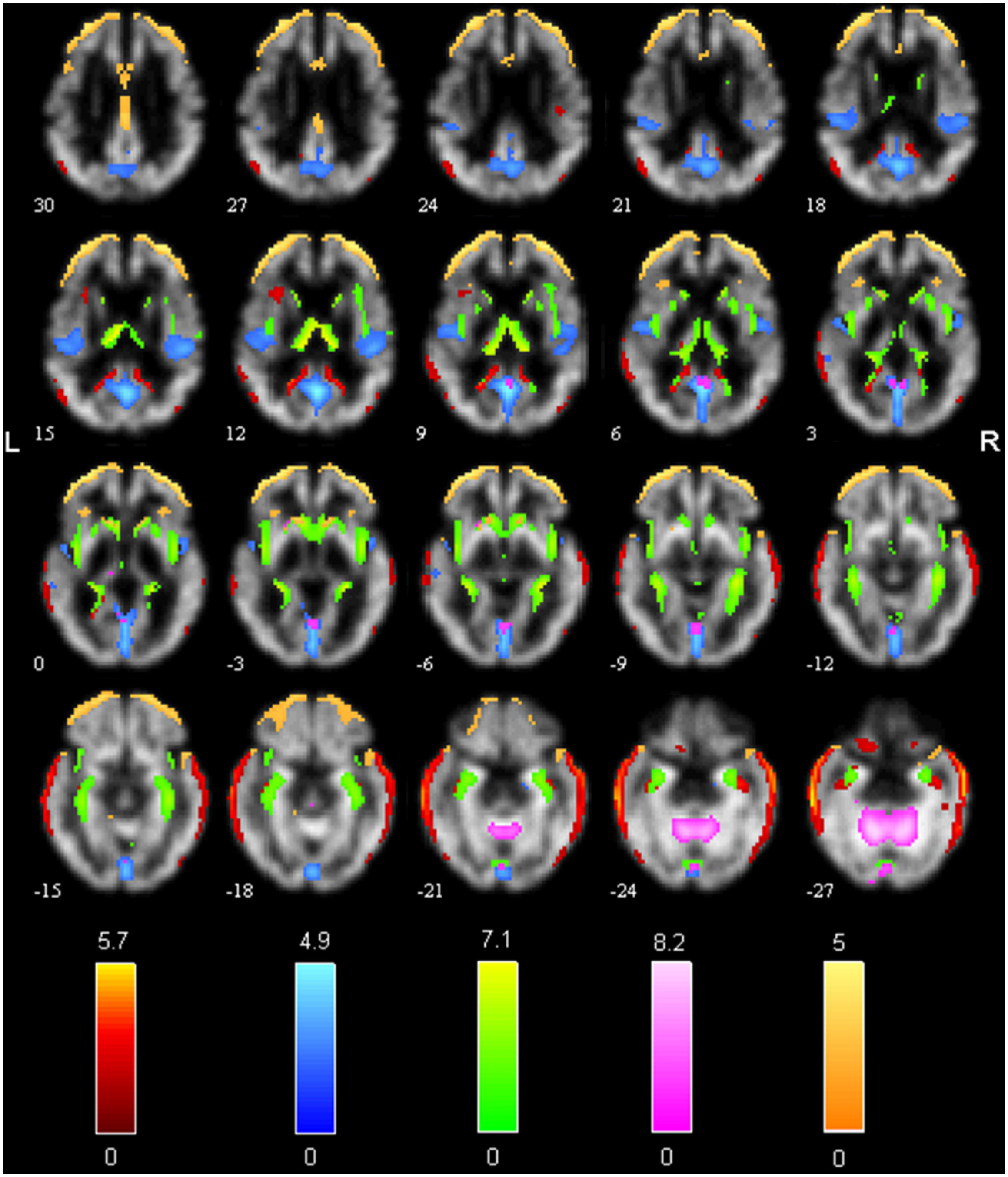

Figure 3. Independent components discovered after ICA. Different colors represent different sources. Red, component 1; blue, component 2; green, component 4; pink, component 11; orange, component 14.

components from the MNI coordinate system to the coordinates of the standard space of Talairach and Tournoux [57]. The transformed coordinates were then inputted into the TalairachClient, a Java application for finding individual and batch labels, which was created and developed by Jack Lancaster and Peter Fox at the Research Imaging Center at the University of Texas Health Science Center, San Antonio, which is available at http://www.talairach.org/. The output of the TalairachClient displayed summarized labels of the components we needed.

Classification

To perform classification, we first needed to determine the appropriate data matrix for train-

Table 3. Talairach labels for regions of significant sources (AD-HC)

Source name	Brodmann area	Volume (mm³)	
		Left	Right
Source 1: Component 4			
Postcentral Gyrus	3, 2, 1, 5, 40, 43	54	37
Superior Temporal Gyrus	22, 21, 41, 38	106	88
Insula	13, 22	121	108
Rectal Gyrus	11	12	13
Sub-Gyral	20, 21, 10, 6, Hip	198	171
Middle Frontal Gyrus	6, 11, 8, 47, 9	69	77
Lingual Gyrus	18, 19	44	54
Extra-Nuclear	13, CC, AC	105	89
Middle Temporal Gyrus	21, 22, 38, 39	38	57
Inferior Parietal Lobule	40	69	60
Thalamus	Pul, AN, VLN, MDN	55	66
Precuneus	7, 31, 23, 19	84	49
Parahippocampal Gyrus	19, 30, 35, 34, 37, Hip, Amy	40	69
Medial Frontal Gyrus	9, 10, 6, 11	144	129
Cingulate Gyrus	32, 24, 31, 23	121	93
Caudate	CH, CB, CT	15	20
Anterior Cingulate	25, 32, 24, 10	57	61
Precentral Gyrus	4, 44, 6, 9	49	51
Superior Parietal Lobule	7	14	13
Supramarginal Gyrus	40	8	10
Cuneus	18, 30, 19, 17, 23, 30	73	51
Inferior Frontal Gyrus	47, 45, 11, 44, 46, 9, 13	122	120
Paracentral Lobule	31, 5, 6, 7	25	18
Superior Frontal Gyrus	8, 9, 6, 11	87	93
Inferior Temporal Gyrus	37, 20, 21	20	14
Transverse Temporal Gyrus	42, 41	11	5
Posterior Cingulate	30, 31, 29	35	12
Uncus	28, 20, 36, Amy	8	21
Subcallosal Gyrus	25, 47	8	1
Fusiform Gyrus	37, 19, 20	33	27
Middle Occipital Gyrus	19, 18	17	11
Orbital Gyrus	11, 47	13	12
Lentiform Nucleus	Pu	4	15
Inferior Occipital Gyrus	18	8	3
Superior Occipital Gyrus	19	4	3
Source 2: Component 2			
Inferior Parietal Lobule	40, 39	72	99
Superior Temporal Gyrus	42, 38, 22, 13, 41, 21, 39	195	175
Postcentral Gyrus	43, 5, 3, 40	65	106
Insula	13, 40, 41	84	101
Inferior Frontal Gyrus	44, 47, 9, 45, 10, 11	58	88
Supramarginal Gyrus	40	29	21
Fusiform Gyrus	37, 19	8	22
Middle Occipital Gyrus	19, 18, 37	78	70
Lingual Gyrus	19, 18, 17	93	76

ing and testing. The number of independent components was estimated, which is represented as N. After ICA, we obtained the mixing matrix A and source matrix S. We figured since we had achieved N different independent components, we had caught N independent source areas at the same time. Common sense dictates that AD and MCI patients suffer greater atrophy of inner brain structures than do HCs [65-68]. As a result, we decided to count our subjects' number of voxels in each source region, and each subject could obtain N different numbers of voxels in different regions. Naturally we get N columns of attributes. We also noticed that each subject of ADNI received a variety of clinical examinations, which is how a value like MMSE was obtained. All these values (to some extent) differentiate patients from HC, and they display a significant evaluation principal in examining and determining the degree of dementia and the duration of disease [69, 70]. Given this consideration, we expanded the attribute matrix with another three columns of attributes: MMSE, GDTOTAL and HMSCORE. Finally, we constructed a new attribute matrix to be used in the following classification and assigned 1 as the label value for one group's components and -1 for the other [71]. In considering the situation that attributes in greater numeric ranges may dominate the classification, we scaled the attribute data. As a

Precuneus	7, 31, 19, 23	136	104
Cingulate Gyrus	31, 24, 32, 23	59	33
Extra-Nuclear	CC	12	24
Posterior Cingulate	30, 31, 29, 23	58	53
Sub-Gyral	21, Hip, CC	38	53
Cuneus	17, 23, 7, 19, 18	147	126
Middle Temporal Gyrus	21, 39, 37, 22, 38, 19	111	194
Superior Parietal Lobule	7	19	19
Precentral Gyrus	4, 6, 9, 44, 43	95	135
Paracentral Lobule	31, 6, 5	17	10
Angular Gyrus	39	12	19
Transverse Temporal Gyrus	42, 41	24	27
Inferior Temporal Gyrus	20, 37, 19	11	16
Anterior Cingulate	32, 24, 25, CC	29	15
Middle Frontal Gyrus	11, 6, 9, 10, 8, 46	51	62
Parahippocampal Gyrus	28, 36, 35, 19, 34, 30, 27, 37	58	61
Superior Occipital Gyrus	19	11	1
Inferior Occipital Gyrus	18, 19	20	8
Uncus	36, 28, 34, 20	5	12
Medial Frontal Gyrus	9, 10, 6, 32, 25, 11	21	35
Superior Frontal Gyrus	10, 8, 6	4	10
Subcallosal Gyrus	34, 25	5	4
Thalamus	Pul	2	4
Rectal Gyrus	11	1	3
Lentiform Nucleus	Pu	0	2
Source 3: Component 14			
Insula	13	66	67
Middle Temporal Gyrus	39, 20, 38, 21, 19	128	127
Inferior Temporal Gyrus	20, 21, 37	32	30
Precuneus	7, 31, 39, 31	34	39
Cingulate Gyrus	24, 23, 31, 32	155	135
Middle Frontal Gyrus	8, 10, 47, 9, 46, 11	298	278
Superior Frontal Gyrus	10, 11, 8, 9	232	259
Medial Frontal Gyrus	9, 10, 25, 11, 6, 25	126	115
Middle Occipital Gyrus	19, 18, 37	30	50
Parahippocampal Gyrus	34, 35, 28, 36, 37, Amy, Hip	48	32
Superior Temporal Gyrus	22, 38, 39, 13	158	182
Precentral Gyrus	6, 4, 9, 44, 13	93	97
Cuneus	19, 18, 17, 23, 30	19	10
Inferior Frontal Gyrus	47, 45, 46, 10, 44, 13, 11, 9	166	138
Sub-Gyral	6, 20, 7, CC	72	86
Extra-Nuclear	13, CC, OT	48	45
Posterior Cingulate	30, 31, 29, 23	35	35
Uncus	36, 28, 34, Amy	40	30
Paracentral Lobule	4, 31, 6	9	4
Orbital Gyrus	11, 47	14	11
Inferior Parietal Lobule	40, 7	58	56
Anterior Cingulate	32, 33, 24, 25, 10	66	67
Lentiform Nucleus	Pu	8	15

result, the training matrix was comprised of 50% of the samples for the following processing. Then we used the other 50% of the attribute matrix as our testing matrix to find out the effectiveness of the model we had generated from the training step. Here, we called on another Matlab toolbox LIBSVM [34, 72], developed by Chih-Jen Lin of the National Taiwan University for help. Two important functions of this SVM toolbox are the use of training data to generate a model and the use of the outcome model to predict the class-belonging of the testing data.

Results

ICA results

We first compared the images between group AD and group HC, and then we compared the images between group MCI and group HC in the same way. The results are explained below.

AD vs. HC

The number of independent components analyzed under the previous estimation was 17. After that, the two-sample t-test was used to detect those significant components, and resulted in six independent components (out of the 17 components) being tested to show a p-value less than 0.05. Then, one component that implied obvious unimportant border information was excluded, and the coordinates of the five remaining components we-

Superior Parietal Lobule	7	9	21
Transverse Temporal Gyrus	42, 41	6	18
Supramarginal Gyrus	40	6	20
Thalamus	MDN, AN, Pul	11	11
Postcentral Gyrus	2, 3, 43, 40, 5, 1, 7, 4	89	65
Rectal Gyrus	11	23	10
Fusiform Gyrus	20, 19, 37	21	20
Angular Gyrus	39	10	14
Lingual Gyrus	18, 17	7	12
Superior Occipital Gyrus	19	7	6
Inferior Occipital Gyrus	18, 17	5	14
Subcallosal Gyrus	25	2	2
Caudate	CH	4	1
Source 4: Component 11			
Thalamus	Pul, VPLN, MDN, VPLN, VLN, MB	32	37
Superior Temporal Gyrus	38, 22, 42	15	50
Precuneus	7, 23, 31, 39	40	20
Precentral Gyrus	4, 6, 44, 3	54	72
Orbital Gyrus	11, 47	0	5
Middle Temporal Gyrus	39, 37, 22, 38, 21, 20	36	57
Medial Frontal Gyrus	9, 11, 10, 6, 8, 25	29	33
Postcentral Gyrus	3, 43, 4, 5, 40, 2, 1, 7	43	67
Cuneus	18, 30, 19, 17, 7	47	47
Middle Frontal Gyrus	9, 6, 11, 8	22	33
Lentiform Nucleus	Pu	5	5
Posterior Cingulate	31, 23, 30	29	13
Cingulate Gyrus	31, 24	35	14
Extra-Nuclear	13	36	44
Superior Frontal Gyrus	11, 9, 6, 8, 10	16	30
Inferior Parietal Lobule	40	25	37
Inferior Frontal Gyrus	47, 11, 45, 44, 9	29	45
Paracentral Lobule	31, 6, 5	7	6
Middle Occipital Gyrus	18	27	24
Uncus	20, 28, Amy	17	17
Lingual Gyrus	18, 19, 17	42	29
Anterior Cingulate	32, 24, 25	18	23
Parahippocampal Gyrus	36, 35, 34, Amy	30	31
Insula	13	8	57
Fusiform Gyrus	20	9	6
Inferior Temporal Gyrus	20, 21, 37	3	10
Caudate	CH	2	3
Inferior Occipital Gyrus	19, 18	10	8
Superior Parietal Lobule	7	2	3
Subcallosal Gyrus	47	1	1
Supramarginal Gyrus	40	4	3
Source 5: Component 1			
Middle Occipital Gyrus	19, 18, 37	67	88
Superior Frontal Gyrus	11, 10, 6, 9, 8	51	73
Medial Frontal Gyrus	25, 6, 10, 32, 8, 9	36	36

re transformed and their Talairach labels summarized. Also, we made the visualization of the five available components, component 1, component 2, component 4, component 11 and component 14, as is shown in **Figure 3**. Their *p*-values can be listed as 1.39×10^{-8}, 2.24×10^{-6}, 0.0024, 0.012, 0.017, respectively, so we can rearrange the five components in ascending order by their *p*-values. As a result, we had five sources representing five different areas that significantly decrease in the gray matter of AD patients' images when compared to HCs.

The detailed Talairach labels of these five sources are listed in **Table 3** in order of increasing *p* values (1.39×10^{-8}, 2.24×10^{-6}, 0.0024, 0.012, 0.017). The areas involved in each source with the corresponding Brodmann area were arranged in the first two columns. The volumes, in cubic millimeter, of the target areas in the left cerebrum and right cerebrum were also displayed in the right two columns.

MCI vs. HC

Using the MIC criteria, the estimated independent components were found to be 11. From these 11 components, components 5 and 10 were two significant components with *p*-values under 0.05 that could be used to differentiate MIC subjects from healthy ones. The visualization of these two components appear in

Precuneus	7, 31, 19, 39	65	80
Middle Temporal Gyrus	21, 22, 19, 37, 39, 38	149	201
Middle Frontal Gyrus	6, 8, 9, 11, 10	83	121
Superior Temporal Gyrus	38, 22, 42, 21, 39	77	116
Angular Gyrus	39	17	29
Inferior Frontal Gyrus	47, 11, 45, 46	29	50
Posterior Cingulate	29, 30, 23	37	33
Parahippocampal Gyrus	36, 19, 30, Hip	12	25
Inferior Parietal Lobule	40, 7	50	28
Inferior Temporal Gyrus	20, 19, 37, 21	43	65
Anterior Cingulate	24, 32	12	12
Thalamus	Pul, VPLN, MDN, MB	19	20
Superior Parietal Lobule	7	12	21
Precentral Gyrus	6, 44, 9, 4	42	36
Sub-Gyral	6, 20, 7, 8, Hip, CC	79	99
Extra-Nuclear	13, CC	11	37
Inferior Occipital Gyrus	18, 19	24	9
Lingual Gyrus	18, 17, 19, 30	13	21
Cingulate Gyrus	31, 24, 32	14	9
Supramarginal Gyrus	40	10	18
Uncus	36, 28, 34, Amy	10	30
Fusiform Gyrus	20, 37	23	33
Rectal Gyrus	11	5	2
Paracentral Lobule	5, 31	13	15
Postcentral Gyrus	2, 3, 40,43, 7	19	27
Orbital Gyrus	11, 47	1	7
Insula	13	19	35
Cuneus	18, 17, 18	40	30
Superior Occipital Gyrus	19	4	12
Caudate	CT	0	1

Abbreviations: AC = Anterior Commissure, Amy = Amygdala, AN = Anterior Nucleus, CB = Caudate Body, CC = Corpus Callusum, CH = Caudate Head, CT = Caudate Tail, Hyp = Hpyothalamus, Hip = Hippocampus, LGP = Lateral Globus Pallidus, MB = Mamillary Body, MDN = Medial Dorsal Nucleus, OT = Optic Tract, Pu = Putamen, Pul = pulvinar, VLN = Ventral Lateral Nucleus, VPLN = Ventral Posterior Lateral Nucleus.

Figure 4, and the Talairach label of each is summarized in **Table 4**.

Classification results

Since we randomly chose 50% of the samples for training, a different dataset consisting of different subjects may result in different outcomes. To handle this, we carried out the classification multiple times so that we could get the statistically averaged value. **Figure 5** displays the results of our 100 analyses in two sets of comparisons, and in **Table 5**, the part of independent components and clinical measurements (ICs+CLI) display the averaged values of accuracy, sensitivity, and specificity. The number of true positives (TP) denote the number of patients correctly classified; TN, the number of true negatives; FP, the number of false positives; and FN, the number of false negatives, with the classification accuracy defined as accuracy = (TP+TN)/(TP+FP+TN+FN), in which the specificity is defined as sensitivity = TP/(TP+FP), and the sensitivity as specificity = TN/(TN+FN).

Discussion

Why ICA?

Our summarized results are as follows: first, the volume of gray matter in both MCI subjects and AD patients' brains had declined, with the difference being that the AD patients' group had a greater decline. Second, the Talairach labels anatomically implied that (compared to healthy people) MCI subjects suffered gray matter loss mainly in the cerebellar tonsil, culmen, tuber, declive, inferior semi-lunar lobule, uvula and fusiform gyrus, while AD patients also lost gray matter in areas like the parahippocampal gyrus, posterior cingulate, temporal gyrus, and so on. Our results were consistent using our research approaches, but compared to previous studies. One difference experienced was that the lost gray matter in MCI that is, to some extent, the preliminary stage of AD. Third, since we have achieved the detailed Talairach labels of the declined areas, it is possible for related experts to do more in-depth research in the field.

We have made clear that the clinical examination value like MMSE is a significant indicator of the clinical diagnosis of dementia. So the

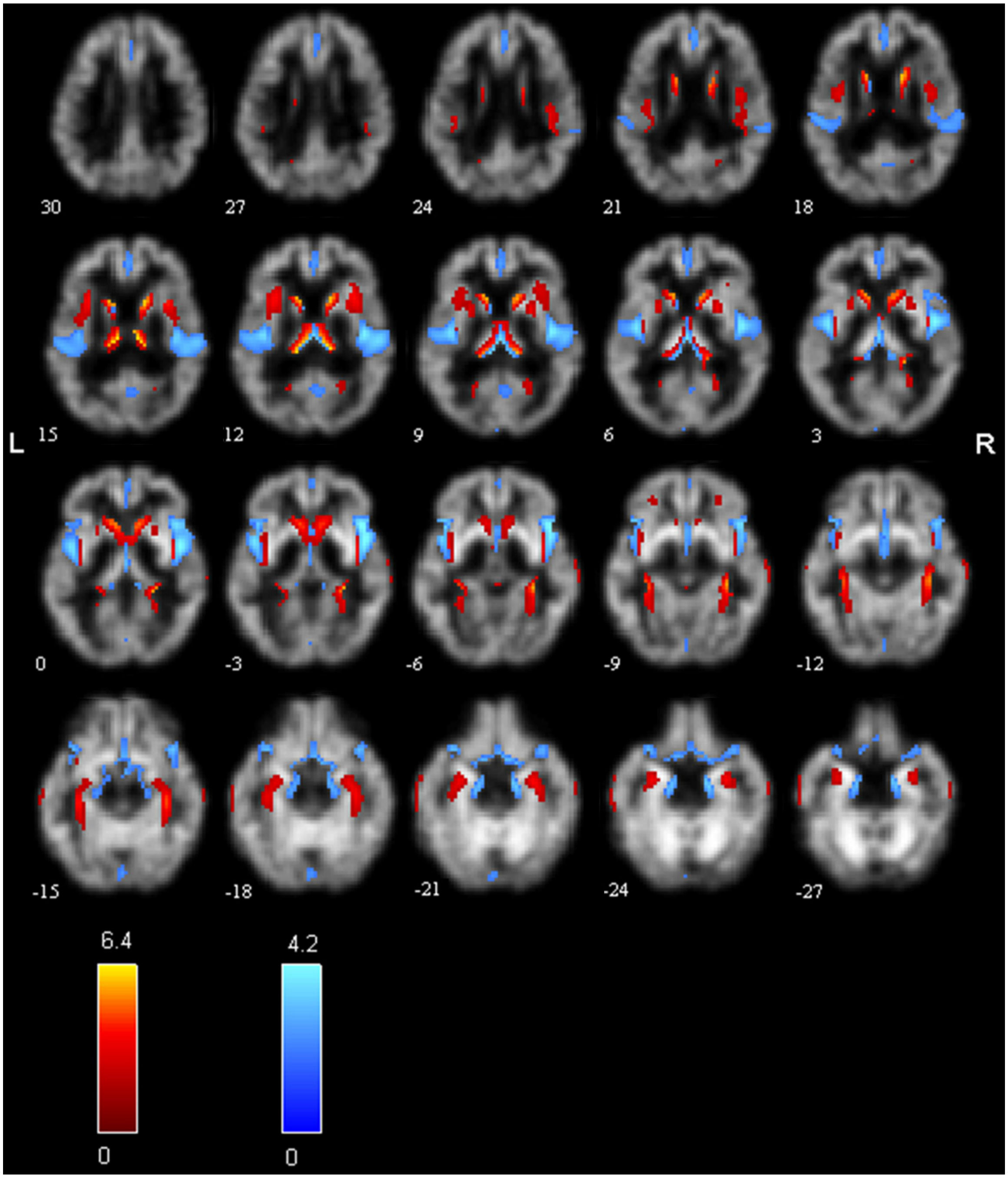

Figure 4. Sources discovered between groups MCI and HC. Red, component 5; blue, component 10.

questions are: how can those results express the effect of ICA? Is there a possibility that it is those clinical examination gains that have highlighted our classification accuracy? The following discussion shows our results. We took off the columns of voxel numbers from the attribute data matrix and re-constructed it with just three columns: MMSE, GDTOTAL, and HMSCORE [69, 70]. Labeled as it had been before, the training matrix was built by randomly picking 50% of the rows of attributes from the new data matrix. A new model came out after training these data, and then the whole matrix was entered into the predictive function of LIBSVM. Similarly, to get rid of the exceptional case, depending on single specific prediction, we summed up 100 results and statistically averaged the value of all these 100 cases in **Figure 6**. This allowed us to come up with the average accuracy, specificity, and sensitivity at

Table 4. Talairach labels for regions of significant sources (MCI-HC)

Source name	Brodmann area	Volume (cmm)	
		Left	Right
Source 1: Component 5			
Middle Frontal Gyrus	8, 11, 6, 9, 10, 46, 47	176	139
Inferior Frontal Gyrus	47, 9, 45, 11, 13, 44	124	115
Caudate	CT, CB, CH	34	40
Parahippocampal Gyrus	19, 30, 20, 37, 36, Amy, Hip	63	79
Thalamus	Pul, AN, MDN, LPN, VAN	63	63
Posterior Cingulate	31, 30, 29	24	25
Postcentral Gyrus	3, 2, 40, 5, 43	63	76
Middle Temporal Gyrus	21, 22, 39, 37	102	127
Cuneus	17, 30, 19	35	51
Fusiform Gyrus	19, 37, 20, 18	75	63
Superior Frontal Gyrus	6, 11, 9, 8, 10	169	123
Paracentral Lobule	5, 31, 6	24	28
Cingulate Gyrus	24, 32, 9, 31	38	30
Inferior Temporal Gyrus	20, 37, 21	50	38
Anterior Cingulate	32, 25, 10, 24	51	48
Extra-Nuclear	13, AC, CC, OT	165	140
Insula	13	138	137
Medial Frontal Gyrus	9, 8, 11, 10, 32, 6, 25	176	199
Rectal Gyrus	11	23	19
Sub-Gyral	21, 20, 6, 10, 13, 8, Hip, CC	264	185
Lingual Gyrus	18, 17, 19	63	37
Superior Temporal Gyrus	22, 38, 42	133	135
Precentral Gyrus	6, 4, 9, 44	112	95
Lentiform Nucleus	Pu, LGP	17	27
Transverse Temporal Gyrus	41, 42	12	14
Inferior Parietal Lobule	40, 39	86	93
Precuneus	31, 7, 19	51	55
Middle Occipital Gyrus	19, 37, 18	39	28
Uncus	28, 36, Amy	8	20
Supramarginal Gyrus	40	2	16
Superior Parietal Lobule	7	15	12
Orbital Gyrus	47, 11	19	18
Angular Gyrus	39	4	3
Superior Occipital Gyrus	19	1	4
Inferior Occipital Gyrus	18, 19	6	11
Subcallosal Gyrus	25	5	8
Source 2: Component 10			
Cingulate Gyrus	32, 31, 24	61	37
Sub-Gyral	21, 13, CC, Hip	67	78
Anterior Cingulate	32, 25, 24, 10	61	55
Insula	13, 40	81	117
Transverse Temporal Gyrus	41, 42	24	29
Posterior Cingulate	23, 31, 30, 29	53	44
Precuneus	31, 7, 23, 19	99	100
Superior Temporal Gyrus	22, 38, 41, 42, 21, 39	242	179

Parahippocampal Gyrus	34, 28, 30, 35, 36, 27, 35, 19, Hip, Amy	112	72
Paracentral Lobule	31, 6, 5, 31	18	17
Cuneus	19, 17, 18, 30, 7, 23	101	81
Middle Frontal Gyrus	9, 6, 10, 46, 11, 8	65	61
Fusiform Gyrus	19, 18, 20, 37	29	33
Inferior Frontal Gyrus	47, 9, 44, 47,46, 45, 11	174	122
Middle Temporal Gyrus	22, 21, 19, 39, 38	112	132
Extra-Nuclear	CC, AC	60	50
Precentral Gyrus	6, 4, 43, 44, 9	86	97
Superior Frontal Gyrus	10, 8, 11	52	43
Postcentral Gyrus	3, 40, 2, 43, 5	97	78
Medial Frontal Gyrus	9, 10, 6, 11, 8, 25	145	79
Middle Occipital Gyrus	18, 19, 37	19	30
Uncus	34, 28, 36, 20, 36	37	15
Lingual Gyrus	17, 18, 19	70	59
Inferior Parietal Lobule	40	75	50
Thalamus	Pul, MDN, LPN, VAN	24	23
Inferior Temporal Gyrus	20, 37	11	17
Subcallosal Gyrus	25, 34	7	6
Caudate	CH, CB	16	23
Supramarginal Gyrus	40	32	7
Rectal Gyrus	11	24	21
Orbital Gyrus	11, 47	22	13
Inferior Occipital Gyrus	17, 18	8	25
Lentiform Nucleus	Pu, LGP	1	5
Superior Parietal Lobule	7	2	6
Superior Occipital Gyrus	19	1	6
Angular Gyrus	39	1	6

a similarly high level, with sensitivity at almost an identical level. The averaged accuracy, sensitivity, and specificity after testing under this circumstance turned out to be 96.7%, 96.5%, and 96.9% for group AD, and 79.5%, 74.0%, 85.1% for group MCI using only CLI, compared to 97.7%, 99.2%, 96.2% for groups AD and HC, and 87.8%, 86.0%, 89.6% for groups MCI and HC using both ICs and CLI. The latter's relative poorer accuracy implied that classification relying on the clinical examination values are unilateral and not all-inclusive. The ICA section of our trial provided better classification capabilities. The averaged results of all those 100 experiments can be found in **Table 5** in which classifications between AD and HC, as well as MCI and HC, were both displayed. According to a different training set, **Table 5** was divided into three parts. In the Only ICs part, we showed the classification accuracy using only the numbers of voxels in each component region based on ICA, while in the second part the Only CLI were results of merely clinical measurements. The last one, the ICs+CLI, resulted from a combination of both feature sources. In **Figure 7** we displayed the accuracy values of these three parts for better visualization.

We have chosen MIC as our independent component estimation criterion. To testify its superiority, we also used AIC and MDL to estimate the number of independent components between group AD and group HC, and it turned out to be 34 of AIC and 17 of MDL. As MDL shared the same independent component number, the significant components by the two sample t-test was also the same, since AIC showed great deviation from MIC in the resulting numbers. We imposed the same post-procedures to analyze the dataset, and components 2, 4, 5, 6, 8, 9, 11, 16, 19, 20, 22,

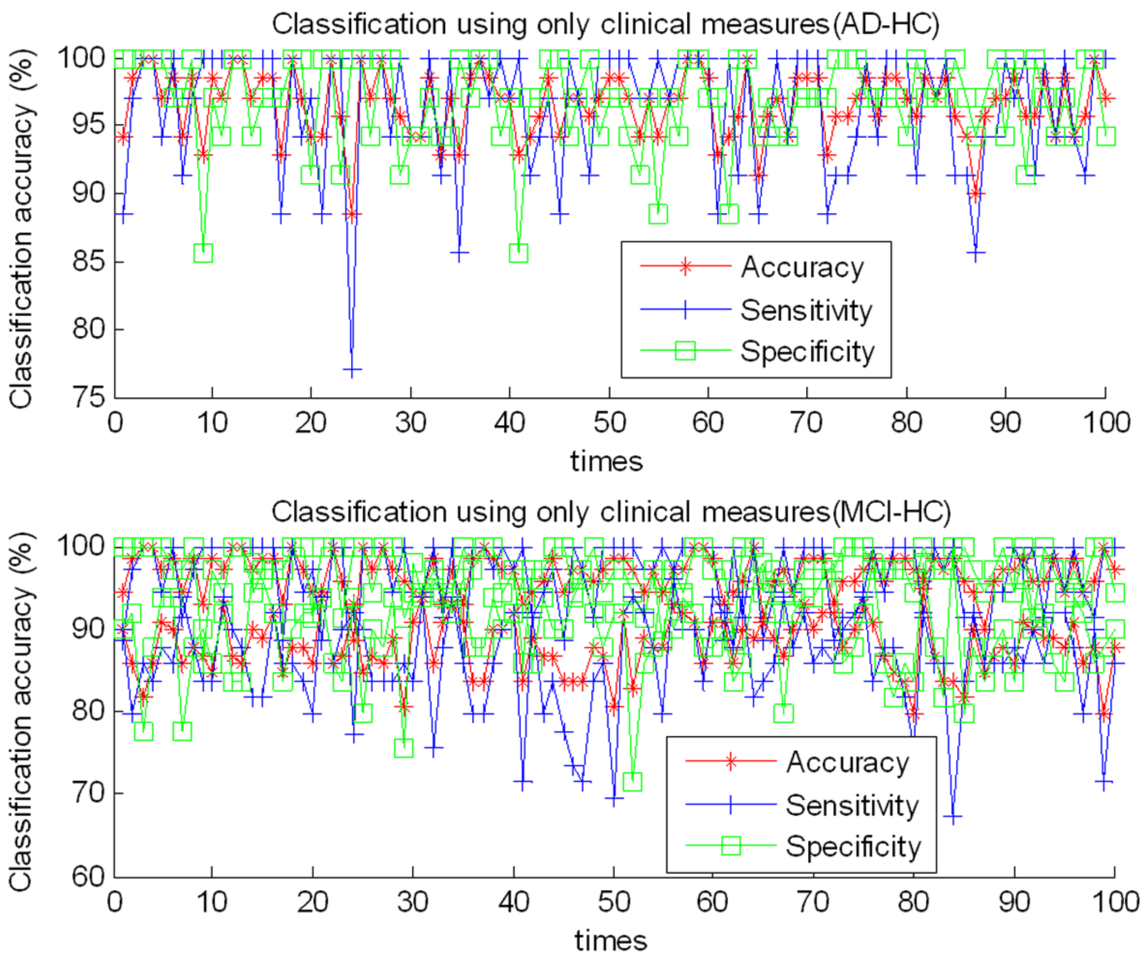

Figure 5. The classification accuracy, sensitivity, and specificity of 100 tests.

Table 5. Classification accuracy of AD or MCI from healthy controls

Training Sets	Parameters	AD vs. HC (mean ± sd)	MCI vs. HC (mean ± sd)
Only ICs	Accuracy	93.6 ± 2.4	85.3 ± 2.4
	Sensitivity	94.3 ± 3.8	82.1 ± 4.8
	Specificity	93.0 ± 3.8	88.6 ± 5.0
Only CLI	Accuracy	96.7 ± 2.0	79.5 ± 2.5
	Sensitivity	96.5 ± 3.8	74.0 ± 4.8
	Specificity	96.9 ± 2.4	85.1 ± 6.2
ICs+CLI	Accuracy	97.7 ± 0.8	87.8 ± 2.7
	Sensitivity	99.2 ± 0.7	86.0 ± 4.5
	Specificity	96.2 ± 1.5	89.6 ± 4.4

23, 24, 25, 26, 27, 28, 29 and 33 showed more of a difference between the two engaged groups. To get a clear visualization, here, we showed components 4, 5, 20, 24, and 33, which corresponded to the smallest five *p* values compared to other components in **Figure 8**. Therefore, it was not hard to find that the resulting area was mostly compatible in the MIC result and in the AIC result. What we could draw out was that the AIC result was suggestive of more artifacts, such as showing sharp edges (e.g. component 2 with larger *p* value) appearing mainly in regions that do not contain gray matter (e.g. white matter or ventricles), and so on.

In using structural MRI images for classification between AD, MCI and HC, researchers like Fan [34, 35, 73] extracted voxel-wise tissue probability as features for classification. Cortical thickness [74-76] was another source of features and was used in certain research. Hippocampal volumes of subjects were calculated and applied into classification as a feature by researchers like Gerardin [77, 78]. It can be revealed from this research that regi-

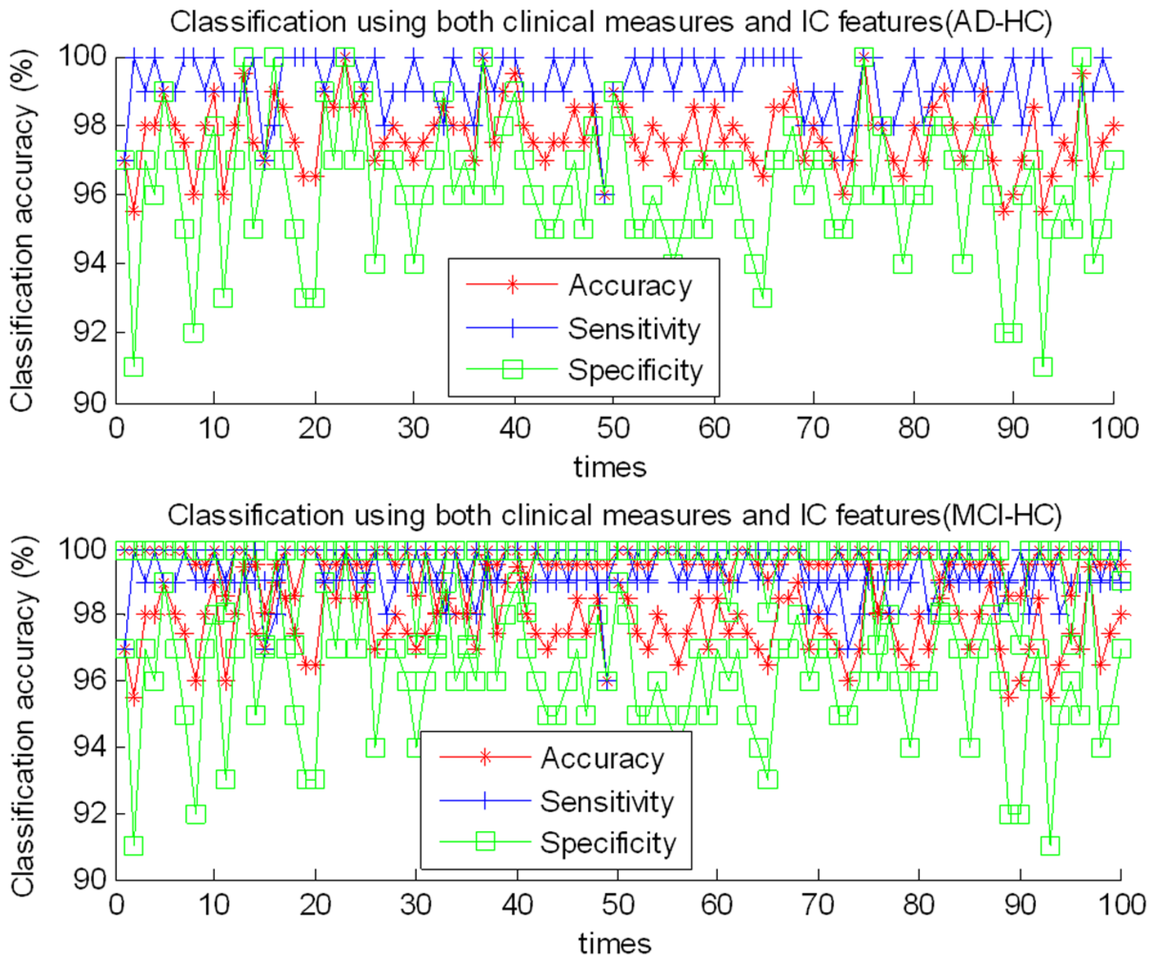

Figure 6. The classification accuracy, sensitivity, and specificity of 100 tests using only clinical measures.

ons such as the hippocampus, amygdala, entorhinal cortex, uncus, temporal pole and parahippocampal regions are the top regions that are selected and closely interrelated to AD [79-81]. However, in this research, each only used partial information of these regions and therefore it could be improved upon. Besides, with sMRI and other modalities such as PET, the CSF also contains complementary information for the diagnosis of AD. Reports of combining biomarkers from different modalities have been released. Among them, there were some practices concatenating all features from different modalities into a larger feature matrix [82, 83]. Researchers like Ye and Zhang [24, 84] further developed this method by using a kernel combination method to construct biomarkers from different modalities into a unified feature matrix. We can see that these recent ways, to a certain extent, take into better consideration features that could differentiate groups by combining more information of different modalities to reveal better results. The method we propose here considers almost all of the interested regions mentioned above that can be discovered from the table by way of ICA. Moreover, integrated with commonly used clinical measures, this method showed more satisfactory results. A future consideration is to use amethod that can explore the values of voxels and their numbers in those interested regions, and modify the way we comb values to extract both voxels and clinical measures.

Conclusion

In our study, we aimed to find innovative and useful information between AD patients and HC patients, and between MCI subjects and

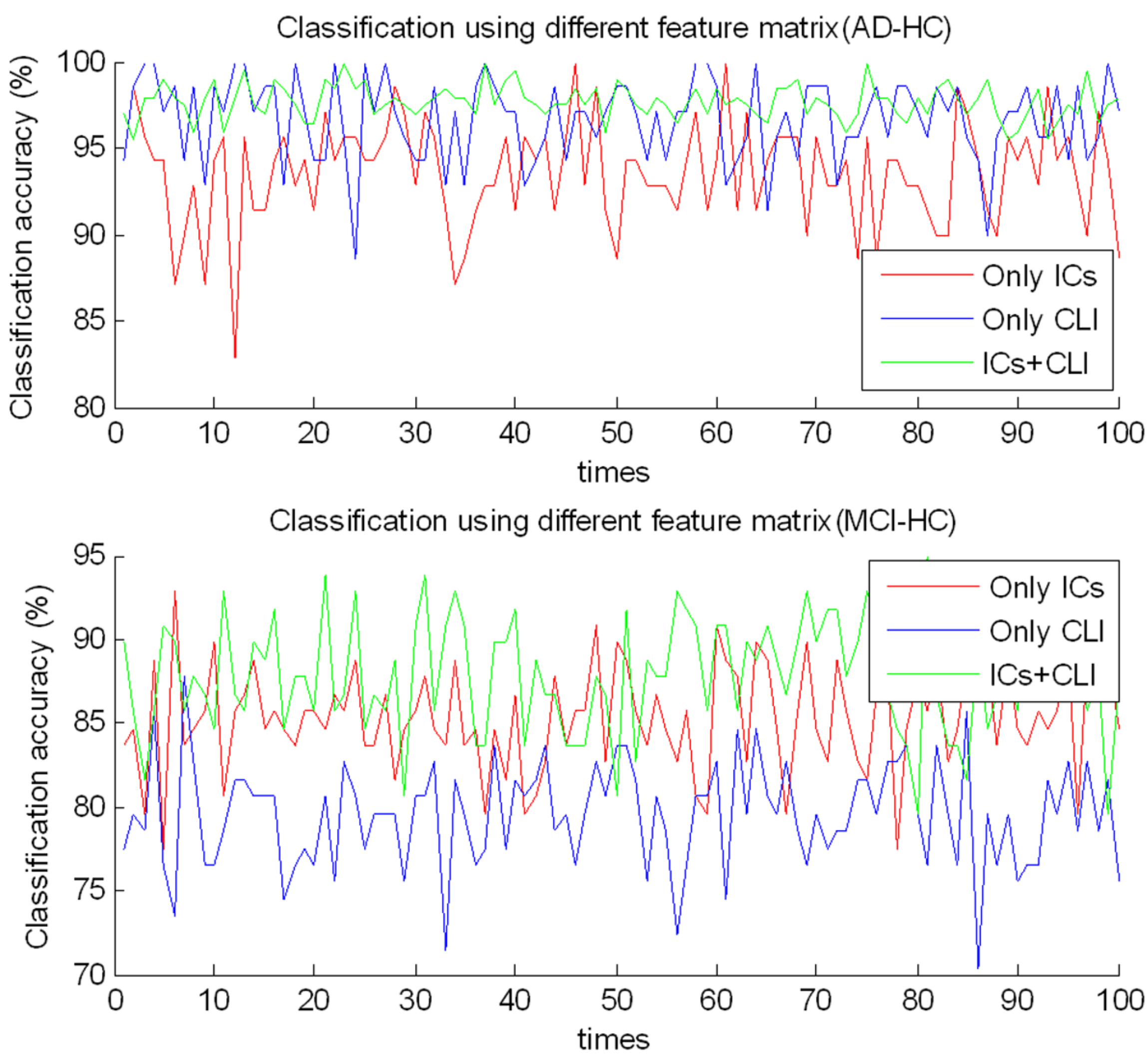

Figure 7. Comparison among three classifications using different feature matrix. Only ICs: classification accuracy using only the numbers of voxels in each component region based on ICA; Only CLI: only clinical measurements were used to construct feature matrix; ICs+CLI: accuracy came out of the combination of both feature sources.

HC subjects. To reach this goal, we set up our experimental process using the following steps: first, the pre-processing stage involved a set of conducts being applied to the subject dataset in order to make sure that all the data in the following steps met the IID requirement. Then we extracted the biological characters using ICA (or we can call this analyzing method SBM). Compared with VBM, it is a multi-covariate approach that takes the spatial information among coherent voxels into consideration. Before we actually executed ICA, we compared several common ITC and chose MIC to perform the independent components estimation. After all these, we analyzed the specific components that had been drawn out from the dataset and obtained visualization and gathered the Talairach labels of all the significant sources. Lastly, we extracted features that significantly differentiated groups and classified them. The results we obtained reveal that AD patients' brains change mostly in the areas of the hippocampus, amygdala, and so on, as some research has already revealed. MCI subjects also experience brain tissue loss, but the volume of gray matter lost is far less, indicating that MCI is, to some extent, the previous stage of AD. Since we are not professionals in psychiatry, the conclusions we can draw are limited. What we find gratifying is that our results are consistent with already-known research conclusions and can be additionally

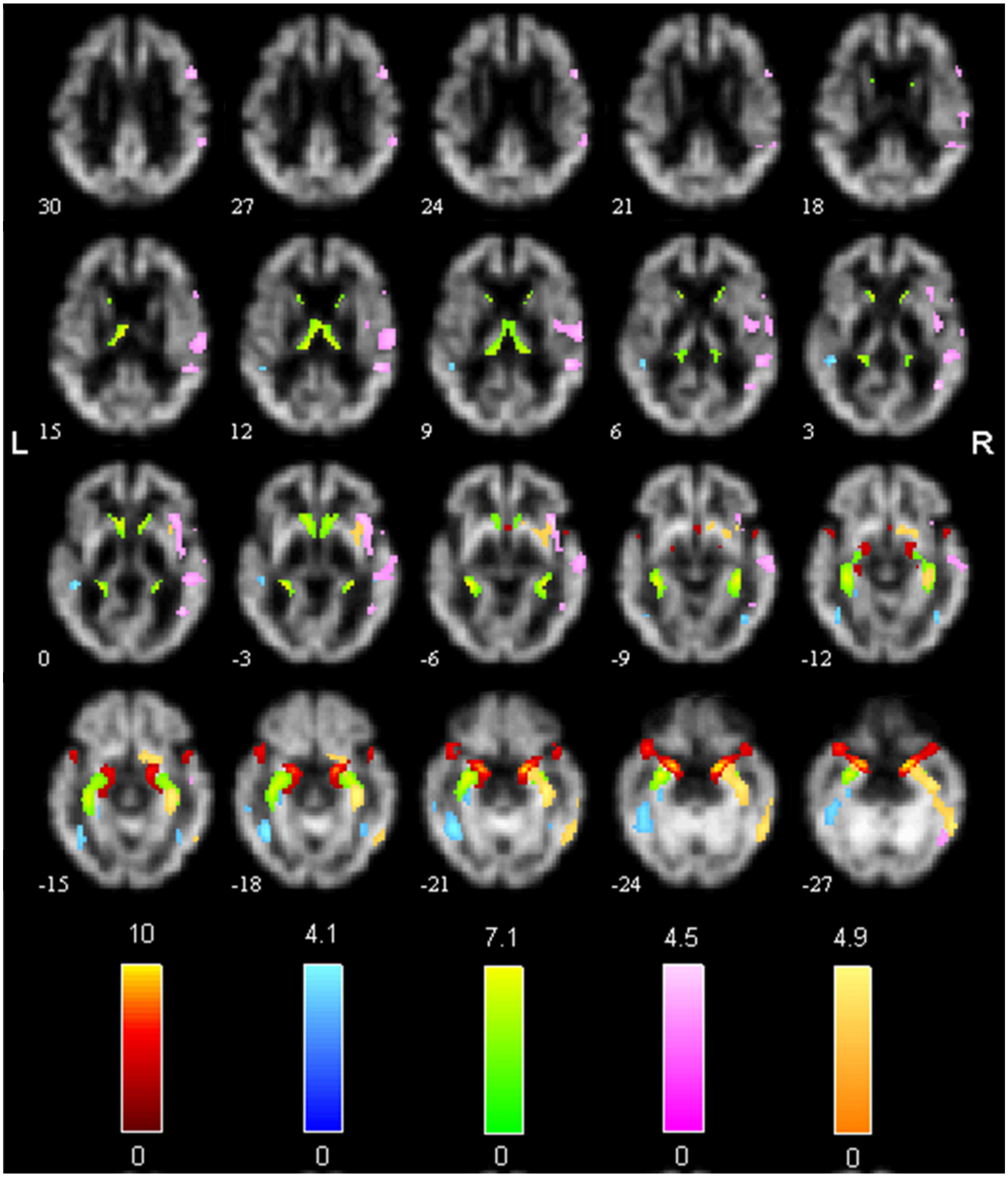

Figure 8. Components 4, 5, 20, 24, and 33 using AIC to estimate the number of independent components.

helpful. ICA was brought into morphometry analysis, making it multivariate to better consider spatial information among the neighboring voxels clustered in one source. MIC applied in our independent components estimation before ICA showed better results in terms of the number of independent components.The final classification revealed that ICA was a potentially useful approach to analyze MRIs and to extract the features we needed.

Acknowledgements

The authors would like to express their gratitude for the support from the Shanghai Maritime University (Grant No. 20090175 to WY), and for the NIH grant (R01 AG056614 to XH).

Data collection and sharing for this project was funded by the Alzheimer's Disease Neuroimaging Initiative (ADNI) (National Institutes of Health Grant U01 AG024904) and DOD ADNI (Department of Defense awardnumber W81XWH-12-2-0012). ADNI is funded by the National Institute on Aging, the National Institute of Biomedical Imaging and Bioengineering, and through generous contributions from the following: AbbVie, Alzheimer's Association; Alzheimer's Drug Discovery Foundation; Araclon Biotech; Bio Clinica, Inc.; Biogen; Bristol-Myers Squibb Company; CereSpir, Inc.; Cogstate; Eisai Inc.; Elan Pharmaceuticals, Inc.; Eli Lilly andCompany; EuroImmun; F. Hoffmann-La Roche Ltd and its affiliated company Genentech, Inc.; Fujirebio; GE Health care; IXICO Ltd.; Janssen Alzheimer Immunotherapy Research & Development, LLC.; Johnson & Johnson Pharmaceutical Research & Development LLC.; Lumosity; Lundbeck; Merck & Co., Inc.; MesoScale Diagnostics, LLC.; NeuroRx Research; Neurotrack Technologies; Novartis Pharmaceuticals Corporation; Pfizer Inc.; Piramal Imaging; Servier; Takeda Pharmaceutical Company; and Transition Therapeutics. The Canadian Institutes of Health Research is providing funds to support ADNI clinical sitesin Canada. Private sector contributions are facilitated by the Foundation for the National Institutes of Health (www.fnih.org). The grantee organization is the Northern California Institute for Research and Education, and the study is coordinated by the Alzheimer's Therapeutic Research Institute at the University of Southern California. ADNI data are disseminated by the Laboratory for Neuro Imaging at the University of Southern California.

Disclosure of conflict of interest

None.

Address correspondence to: Dr. Xudong Huang, Neurochemistry Laboratory, Department of Psychiatry, Massachusetts General Hospital and Harvard Medical School, 149 13th Street, Charlestown, MA 02129, USA. Tel: 617-724-9778; E-mail: Huang.Xudong@mgh.harvard.edu

References

[1] Braak H and Braak E. [Morphological changes in the human cerebral cortex in dementia]. J Hirnforsch 1991; 32: 277-282.

[2] Small GW, Ercoli LM, Silverman DH, Huang SC, Komo S, Bookheimer SY, Lavretsky H, Miller K, Siddarth P, Rasgon NL, Mazziotta JC, Saxena S, Wu HM, Mega MS, Cummings JL, Saunders AM, Pericak-Vance MA, Roses AD, Barrio JR and Phelps ME. Cerebral metabolic and cognitive decline in persons at genetic risk for Alzheimer's disease. Proc Natl Acad Sci U S A 2000; 97: 6037-42.

[3] Jack CR Jr, Shiung MM, Gunter JL, O'Brien PC, Weigand SD, Knopman DS, Boeve BF, Ivnik RJ, Smith GE, Cha RH, Tangalos EG, Petersen RC. Comparison of different MRI brain atrophy rate measures with clinical disease progression in AD. Neurology 2004; 62: 591-600.

[4] Dickerson BC, Salat DH, Greve DN, Chua EF, Rand-Giovannetti E, Rentz DM, Bertram L, Mullin K, Tanzi RE, Blacker D, Albert MS and Sperling RA. Increased hippocampal activation in mild cognitive impairment compared to normal aging and AD. Neurology 2005; 65: 404-411.

[5] Killiany RJ, Gomez-Isla T, Moss M, Kikinis R, Sandor T, Jolesz F, Tanzi R, Jones K, Hyman BT and Albert MS. Use of structural magnetic resonance imaging to predict who will get Alzheimer's disease. Ann Neurol 2000; 47: 430-439.

[6] Greicius MD, Srivastava G, Reiss AL and Menon V. Default-mode network activity distinguishes Alzheimer's disease from healthy aging: evidence from functional MRI. Proc Natl Acad Sci U S A 2004; 101: 4637-4642.

[7] Sperling R. Functional MRI studies of associative encoding in normal aging, mild cognitive impairment, and Alzheimer's disease. Ann N Y Acad Sci 2007; 1097: 146-155.

[8] Frisoni GB, Fox NC, Jack CR, Scheltens P and Thompson PM. The clinical use of structural MRI in Alzheimer disease. Nat Rev Neurol 2010; 6: 67-77.

[9] Cavedo E, Lista S, Khachaturian Z, Aisen P, Amouyel P, Herholz K, Jack C, Sperling R, Cummings J, Blennow K, O'Bryant S, Frisoni G, Khachaturian A, Kivipelto M, Klunk W, Broich K, Andrieu S, de Schotten MT, Mangin J, Lammertsma A, Johnson K, Teipel S, Drzezga A, Bokde A, Colliot O, Bakardjian H, Zetterberg H, Dubois B, Vellas B, Schneider L and Hampel H. The road ahead to cure Alzheimer's disease: development of biological markers and neuroimaging methods for prevention trials across all stages and target populations. J Prev Alzheimers Dis 2014; 1: 181-202.

[10] Bangen KJ, Restom K, Liu TT, Wierenga CE, Jak AJ, Salmon DP and Bondi MW. Assessment of Alzheimer's disease risk with functional magnetic resonance imaging: an arterial spin labeling study. J Alzheimers Dis 2012; 31: S59-74.

[11] Foster NL, Chase TN, Fedio P, Patronas NJ, Brooks RA, Di Chiro G. Alzheimer's disease: focal cortical changes shown by positron emission tomography. Neurology 1983; 33: 961-5.

[12] Duara R, Grady C, Haxby J, Sundaram M, Cutler NR, Heston L, Moore A, Schlageter N, Larson S and Rapoport SI. Positron emission tomography in Alzheimer's disease. Neurology 1986; 36: 879-87.

[13] Silverman DH, Small GW, Chang CY, Lu CS, Kung De Aburto MA, Chen W, Czernin J, Rapoport SI, Pietrini P, Alexander GE, Schapiro MB, Jagust WJ, Hoffman JM, Welsh-Bohmer KA, Alavi A, Clark CM, Salmon E, de Leon MJ, Mielke R, Cummings JL, Kowell AP, Gambhir SS, Hoh CK, Phelps ME. Positron emission tomography in evaluation of dementia-regional brain metabolism and long-term outcome. JAMA 2001; 286: 2120-7.

[14] Marcus C, Mena E and Subramaniam RM. Brain PET in the diagnosis of Alzheimer's disease. Clin Nucl Med 2014; 39: e413-426.

[15] Jack CR Jr, Petersen RC, O'Brien PC and Tangalos EG. MR-based hippocampal volumetry in the diagnosis of Alzheimer's disease. Neurology 1992; 42: 183-188.

[16] Nestor PJ, Fryer TD, Smielewski P and Hodges JR. Limbic hypometabolism in Alzheimer's disease and mild cognitive impairment. Ann Neurol 2003; 54: 343-351.

[17] Greicius MD, Srivastava G, Reiss AL and Menon V. Default-mode network activity distinguishes Alzheimer's disease from healthy aging: evidence from functional MRI. Proc Natl Acad Sci U S A 2004; 101: 4637-4642.

[18] Desikan RS, Sonne F, Fischl B, Quinn BT, Dickerson BC, Blacker D, Buckner RL, Dale AM, Maguire RP, Hyman BT, Albert MS and Killiany RJ. An automated labeling system for subdividing the human cerebral cortex on MRI scans into gyral based regions of interest. Neuroimage 2006; 31: 968-980.

[19] Marshall GA, Lorius N, Locascio JJ, Hyman BT, Rentz DM, Johnson KA and Sperling RA. Regional cortical thinning and cerebrospinal biomarkers predict worsening daily functioning across the Alzheimer disease spectrum. J Alzheimers Dis 2014; 41: 719-728.

[20] Donovan NJ, Wadsworth LP, Lorius N, Locascio JJ, Rentz DM, Johnson KA, Sperling RA and Marshall GA. Regional cortical thinning predicts worsening apathy and hallucinations across the Alzheimer's disease spectrum. Am J Geriatr Psychiatry 2014; 22: 1168-1179.

[21] Chupin M, Gerardin E, Cuingnet R, Boutet C, Lemieux L, Lehericy S, Benali H, Garnero L and Colliot O. Fully automatic hippocampus segmentation and classification in Alzheimer's disease and mild cognitive impairment applied on data from ADNI. Hippocampus 2009; 19: 579-587.

[22] Zhou L, Hartley R, Wang L, Lieby P and Barnes N. Identifying anatomical shape difference by regularized discriminative direction. IEEE Trans Med Imaging 2009; 28: 937-50.

[23] Putcha D, Brickhouse M, O'Keefe K, Sullivan C, Rentz D, Marshall G, Dickerson B and Sperling R. Hippocampal hyperactivation associated with cortical thinning in Alzheimer's disease signature regions in non-demented elderly adults. J Neurosci 2011; 31: 17680-17688.

[24] Zhang D, Wang Y, Zhou L, Yuan H and Shen D. Multimodal classification of Alzheimer's disease and mild cognitive impairment. Neuroimage 2011; 55: 856-867.

[25] Ashburner J, Friston KJ. Voxel-based morphometry-the methods. NeuroImage 2000; 11: 805-821.

[26] Ashburner J and Friston KJ. Voxel-based morphometry-the methods. Neuroimage 2000; 11: 805-821.

[27] Hua X, Gutman B, Boyle CP, Rajagopalan P, Leow AD, Yanovsky I, Kumar AR, Toga AW, Jack CR Jr, Schuff N, Alexander GE, Chen K, Reiman EM, Weiner MW and Thompson PM. Accurate measurement of brain changes in longitudinal MRI scans using tensor-based morphometry. Neuroimage 2011; 57: 5-14.

[28] Hirata Y, Matsuda H, Nemoto K, Ohnishi T, Hirao K, Yamashita F, Asada T, Iwabuchi S and Samejima H. Voxel-based morphometry to discriminate early Alzheimer's disease from controls. Neurosci Lett 2005; 382: 269-274.

[29] Wang WY, Yu JT, Liu Y, Yin RH, Wang HF, Wang J, Tan L, Radua J and Tan L. Voxel-based meta-analysis of grey matter changes in Alzheimer's disease. Transl Neurodegener 2015; 4: 6.

[30] Giesel FL, Thomann PA, Hahn HK and Wilkinson ID. Comparison of manual direct and automated indirect measurement of hippocampus using magnetic resonance imaging. Eur J Radiol 2008; 66: 268-273.

[31] Xu L, Groth KM, Pearlson G, Schretlen DJ and Calhoun VD. Source-based morphometry: the use of independent component analysis to identify gray matter differences with application to schizophrenia. Hum Brain Mapp 2009; 30: 711-724.

[32] Xu L, Pearlson G and Calhoun VD. Joint source based morphometry identifies linked gray and white matter group differences. Neuroimage 2009; 44: 777-789.

[33] Wax M and Kailath T. Detection of signals by information theoretic criteria. IEEE Transactions on Acoustics Speech & Signal Processing 1985; 33: 387-392.

[34] Magnin B, Mesrob L, Kinkingnehun S, Pelegrini-Issac M, Colliot O, Sarazin M, Dubois B, Lehericy S and Benali H. Support vector machine-based classification of Alzheimer's disease from whole-brain anatomical MRI. Neuroradiology 2009; 51: 73-83.

[35] Kloppel S, Stonnington CM, Chu C, Draganski B, Scahill RI, Rohrer JD, Fox NC, Jack CR Jr, Ashburner J and Frackowiak RS. Automatic classification of MR scans in Alzheimer's disease. Brain 2008; 131: 681-689.

[36] Suykens JAK and Vandewalle J. Least squares support vector machine classifiers. Neural Processing Letters 1999; 9: 293-300.

[37] Cauwenberghs G and poggio T. Incremental and decremental support vector machine learning. Neural information Processing Systems 2000; 13: 409-415.

[38] Zhang Y, Dong Z, Phillips P, Wang S, Ji G, Yang J and Yuan TF. Detection of subjects and brain regions related to Alzheimer's disease using 3D MRI scans based on eigenbrain and machine learning. Front Comput Neurosci 2015; 9: 66.

[39] Fung GM and Mangasarian OL. Multicategory proximal support vector machine classifiers. Machine Learning 2005; 59: 77-97.

[40] Jack CR Jr, Bernstein MA, Fox NC, Thompson P, Alexander G, Harvey D, Borowski B, Britson PJ, L Whitwell J, Ward C, Dale AM, Felmlee JP, Gunter JL, Hill DL, Killiany R, Schuff N, Fox-Bosetti S, Lin C, Studholme C, DeCarli CS, Krueger G, Ward HA, Metzger GJ, Scott KT, Mallozzi R, Blezek D, Levy J, Debbins JP, Fleisher AS, Albert M, Green R, Bartzokis G, Glover G, Mugler J, Weiner MW. The Alzheimer's disease neuroimaging Initiative (ADNI): MRI methods. J Magn Reson Imaging 2008; 27: 685-691.

[41] Zhan L, Bernstein MA, Borowski B, Jack CR and Thompson PM. Evaluation of diffusion imaging protocols for the Alzheimer's disease neuroimaging initiative. IEEE International Symposium on Biomedical Imaging 2014; 710-713.

[42] Weiner MW, Veitch DP, Aisen PS, Beckett LA, Cairns NJ, Cedarbaum J, Green RC, Harvey D, Jack CR, Jagust W, Luthman J, Morris JC, Petersen RC, Saykin AJ, Shaw L, Shen L, Schwarz A, Toga AW and Trojanowski JQ. 2014 update of the Alzheimer's disease neuroimaging initiative: a review of papers published since its inception. Alzheimers Dement 2015; 11: e1-120.

[43] Kohannim O, Hua X, Hibar DP, Lee S, Chou YY, Toga AW, Jack CR, Weiner MW and Thompson PM. Boosting power for clinical trials using classifiers based on multiple biomarkers. Neurobiol Aging 2010; 31: 1429-1442.

[44] Schafhitzel T, Rößler F, Weiskopf D and Ertl T. Simultaneous visualization of anatomical and functional 3D data by combining volume rendering and flow visualization. 2007.

[45] Schwarz G. Estimating the dimension of a model. Ann Statist 1978; 6: 461-464.

[46] Al H. A new look at the statistical model identification. Automatic Control IEEE Transactions on 1974; 19: 716-723

[47] Wang G, Ding Q, Sun Y, He L and Sun X. Estimation of source infrared spectra profiles of acetylspiramycin active components from troches using kernel independent component analysis. Spectrochim Acta A Mol Biomol Spectrosc 2008; 70: 571-576.

[48] Williams DB. Comparison of AIC and MDL to the minimum probability of error criterion. Statistical signal and array processing, 1992. Conference proceeding., IEEE Sixth SP Workshop on 1992; 114-117.

[49] Li YO, Adali T and Calhoun VD. Estimating the number of independent components for functional magnetic resonance Imaging data. Human Brain Mapping 2007; 28: 1251-1266.

[50] Wei X, Li YO, Li H, Adali T and Calhoun VD. On ICA of complex-valued fMRI: advantages and order selection. 2008 IEEE International Conference on Acoustics, Speech and Signal Processing 2008; 529-532.

[51] Sekmen AS and Bingul Z. Comparison of algorithms for detection of the number of signal sources. Southeastcon 99 IEEE; 1999: 70-73.

[52] Ashburner J. Computational anatomy with the SPM software. Magnetic Resonance Imaging 2009; 27: 1163-1174.

[53] Abel T, Morabia A and Kohlmann T. New name and new perspectives for the international journal of public health, formerly SPM. Int J Public Health 2007; 52: 1.

[54] Talairach J. Co-planar stereotaxic atlas of the human brain. Thieme Medical 1989.

[55] Calhoun V and Pekar J. When and where are components independent? On the applicability of spatial and temporal ICA to functional MRI data. NeuroImage 2000; 11: 682.

[56] Calhoun VD, Adali T, Hansen LK, Larsen J and Pekar J. ICA of functional MRI data: an overview. International Workshop on Independent Component Analysis & Blind Signal Separation 2003; 281-288.

[57] Rachakonda S, Egolf E, Correa N and Calhoun V. Group ICA of fMRI Toolbox (GIFT) Manual. 2010.

[58] Adeli H, Ghosh-Dastidar S and Dadmehr N. Alzheimer's disease and models of computation: Imaging, classification, and neural models. J Alzheimers Dis 2005; 7: 187-199.

[59] Amari S. Natural gradient learning for over- and under-complete bases in ICA. Neural Computation 1999; 11: 1875-1883.

[60] Hyvärinen A. Independent component analysis: recent advances. Philos Trans A Math Phys Eng Sci 2013; 371: 20110534.

[61] Calhoun V, Adali T and Pearlson G. Independent component analysis applied to fMRI data: a generative model for validating results. IEEE Signal Processing Society Workshop 2004; 37: 509-518.
[62] Calhoun V, Adali T, Pearlson G and Pekar J. A method for making group inferences using independent component analysis of functional MRI data: exploring the visual system. Neuroimage 2001; 13: S88.
[63] Calhoun V, Adali T, Pearlson G and Pekar J. Group ICA of functional MRI data: separability, stationarity and inference. 2001.
[64] Rachakonda S, Egolf E and Calhoun V. Group ICA of fMRI toolbox (GIFT) walk through. 2010.
[65] Apostolova LG, Dutton RA, Dinov ID, Hayashi KM, Toga AW, Cummings JL and Thompson PM. Conversion of mild cognitive impairment to Alzheimer disease predicted by hippocampal atrophy maps. Arch Neurol 2006; 63: 693-699.
[66] Beyer MK, Janvin CC, Larsen JP and Aarsland D. A magnetic resonance imaging study of patients with Parkinson's disease with mild cognitive impairment and dementia using voxel-based morphometry. J Neurol Neurosurg Psychiatry 2007; 78: 254-9.
[67] Apostolova LG and Thompson PM. Mapping progressive brain structural changes in early Alzheimer's disease and mild cognitive impairment. Neuropsychologia 2008; 46: 1597-1612.
[68] Tarawneh R, Head D, Allison S, Buckles V, Fagan AM, Ladenson JH, Morris JC and Holtzman DM. Cerebrospinal fluid markers of neurodegeneration and rates of brain atrophy in early Alzheimer disease. JAMA Neurol 2015; 72: 656-665.
[69] Solomon PR, Adams FA, Groccia ME, DeVeaux R, Growdon JH and Pendlebury WW. Correlational analysis of five commonly used measures of mental status/functional abilities in patients with Alzheimer disease. Alzheimer Dis Assoc Disord 1999; 13: 147-50.
[70] Solomon TM, deBros GB, Budson AE, Mirkovic N, Murphy CA and Solomon PR. Correlational analysis of 5 commonly used measures of cognitive functioning and mental status. Am J Alzheimers Dis Other Demen 2014; 29: 718-22.
[71] Chang DJ, Zubal IG, Gottschalk C, Freeman J, Necochea A, Stokking R, Studholme C, Corsi M, Spencer SS and Blumenfeld H. Statistical parametric mapping: a new approach to analysis of ictal SPECT scans in temporal lobe epilepsy compared to conventional difference imaging. Society for Neuroscience Abstracts 2001; 27: 1464.
[72] Chang CC and Lin CJ. LIBSVM: a library for support vector machines. ACM Transactions on Intelligent Systems and Technology (TIST) 2011; 2: 27.
[73] Fan Y, Shen D, Gur RC, Gur RE, Davatzikos C. COMPARE: classification of morphological patterns using adaptive regional elements. IEEE Trans Med Imaging 2007; 26: 93-105.
[74] Desikan RS, Cabral HJ, Hess CP, Dillon WP, Glastonbury CM, Weiner MW, Schmansky NJ, Greve DN, Salat DH, Buckner RL, Fischl B; Alzheimer's Disease Neuroimaging Initiative. Automated MRI measures identify individuals with mild cognitive impairment and Alzheimer's disease. Brain 2009; 132: 2048-2057.
[75] Lerch JP, Pruessner J, Zijdenbos AP, Collins DL, Teipel SJ, Hampel H, Evans AC. Automated cortical thickness measurements from MRI can accurately separate Alzheimer's patients from normal elderly controls. Neurobiol Aging 2008; 29: 23-30.
[76] Querbes O, Aubry F, Pariente J, Lotterie JA, Démonet JF, Duret V, Puel M, Berry I, Fort JC, Celsis P; Alzheimer's Disease Neuroimaging Initiative. Early diagnosis of Alzheimer's disease using cortical thickness: impact of cognitive reserve. Brain 2009; 132: 2036-2047.
[77] Gerardin E, Chetelat G, Chupin M, Cuingnet R, Desgranges B, Kim HS, Niethammer M, Dubois B, Lehericy S, Garnero L, Eustache F and Colliot O. Multidimensional classification of hippocampal shape features discriminates Alzheimer's disease and mild cognitive impairment from normal aging. Neuroimage 2009; 47: 1476-1486.
[78] Mark JW, Claudia HK, Walter FS, Gay LR and Juan CT. Hippocampal neurons in pre-clinical Alzheimer's disease. Neurobiol Aging 2004; 25: 1205-1212.
[79] Convit A, de Asis J, de Leon MJ, Tarshish CY, De Santi S, Rusinek H. Atrophy of the medial occipitotemporal, inferior, and middle temporal gyri in non-demented elderly predict decline to Alzheimer's disease. Neurobiol Aging 21: 19-26.
[80] Chételat G, Desgranges B, de la Sayette V, Viader F, Eustache F and Baron JC. Mapping gray matter loss with voxel-based morphometry in mild cognitive impairment. Neuroreport 2002; 13: 1939-1943.
[81] Jack CR Jr, Petersen RC, Xu YC, O'Brien PC, Smith GE, Ivnik RJ, Boeve BF, Waring SC, Tangalos EG and Kokmen E. Prediction of AD with MRI-based hippocampal volume in mild cognitive impairment. Neurology 1999; 52: 1397-1403.
[82] Bouwman FH, Schoonenboom SN, van der Flier WM, van Elk EJ, Kok A, Barkhof F, Blankenstein MA, Scheltens P. CSF biomarkers and medial temporal lobe atrophy predict demen-

tia in mild cognitive impairment. Neurobiol Aging 2007; 28: 1070-1074.

[83] Fan Y, Resnick SM, Wu X and Davatzikos C. Structural and functional biomarkers of prodromal Alzheimer's disease: a high-dimensional pattern classification study. Neuroimage 2008; 41: 277-285.

[84] Ye J, Chen K, Wu T, Li J, Zhao Z, Patel R, Bae M, Janardan R, Liu H, Alexander G and Reiman E. Heterogeneous data fusion for alzheimer's disease study. Proceedings of the 14th ACM SIGKDD International Conference on Knowledge discovery and Data Mining 2008; 1025-1033.